A multi-method assessment of the regional sensitivities between flight altitude and short-term O3 climate warming from aircraft NOx emissions

Maruhashi, J.; Mertens, M.; Grewe, V.; Dedoussi, I.C.

DOI
10.1088/1748-9326/ad376a

Publication date
2024

Document Version
Final published version

Published in
Environmental Research Letters

ENVIRONMENTAL RESEARCH
LETTERS

LETTER • OPEN ACCESS

A multi-method assessment of the regional sensitivities between flight altitude and short-term O_3 climate warming from aircraft NO_x emissions

To cite this article: Jin Maruhashi *et al* 2024 *Environ. Res. Lett.* **19** 054007

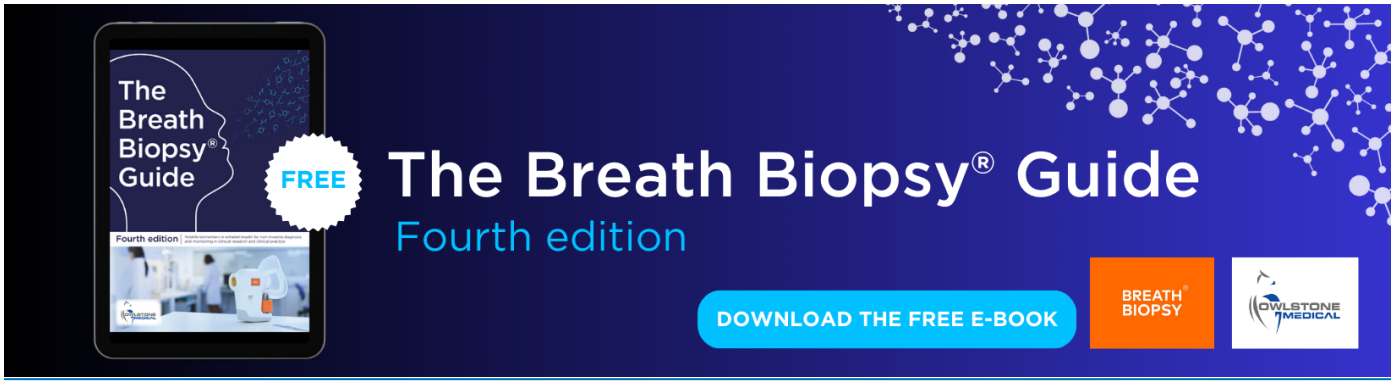

ENVIRONMENTAL RESEARCH
LETTERS

LETTER

A multi-method assessment of the regional sensitivities between flight altitude and short-term O_3 climate warming from aircraft NO_x emissions

Jin Maruhashi[1], Mariano Mertens[2], Volker Grewe[1,2] and Irene C Dedoussi[1,*]

[1] Section Aircraft Noise and Climate Effects, Faculty of Aerospace Engineering, Delft University of Technology, Delft, The Netherlands
[2] Deutsches Zentrum für Luft- und Raumfahrt (DLR), Institut für Physik der Atmosphäre, Oberpfaffenhofen, Germany
[*] Author to whom any correspondence should be addressed.

E-mail: i.c.dedoussi@tudelft.nl

Keywords: NO_x emissions, ozone, aviation climate effects, Eulerian & Lagrangian modeling, tagging, perturbation, flight altitude

Supplementary material for this article is available online

OPEN ACCESS

RECEIVED
9 November 2023

REVISED
20 February 2024

ACCEPTED FOR PUBLICATION
25 March 2024

PUBLISHED
12 April 2024

Abstract

Flight altitude is relevant to the climate effects resulting from aircraft emissions. Other research has shown that flying higher within the troposphere leads to larger warming from O_3 production. Aircraft NO_x emissions are of particular interest, as they lead to warming via the short-term production of O_3, but also to reduced warming via processes like CH_4 depletion. We focus on short-term O_3 production, as it constitutes one of aviation's largest warming components. Understanding how O_3 formation varies altitudinally throughout the upper troposphere/lower stratosphere is essential for designing climate-compatible aircraft and routing. We quantify this variation by performing simulations with a global atmospheric chemistry model for three representative cruise altitudes, five regions and two seasons using three methods: Eulerian tagging, perturbation and Lagrangian tagging. This multi-method, regional approach overcomes limitations of previous studies that utilize only one of these methods and apply global emission inventories biased towards present-day flight distributions, thus limiting their applicability to future aviation scenarios. Our results highlight that underrepresenting emissions in areas with growing flight activity (e.g. Asia Pacific) may lead to significant, regional underestimations of the altitudinal sensitivity of short-term NO_x-related O_3 warming effects in certain cases. We find that emitting in Southern regions, like Australasia, leads to warming larger by a factor of two when compared to global averages. Our findings also suggest that flying lower translates to lower warming from short-term O_3 production and that this effect is strongest during the local summer. We estimate differences ranging from a factor of 1.2–2.6 between tagging and perturbation results that are attributable to non-linearities of NO_x-O_3 chemistry, and derived regional correction factors for a widely-used sub-model. Overall, we stress that a combination of all three methods is necessary for a robust assessment of aviation climate effects as they address fundamentally different questions.

1. Introduction

Aircraft emissions trigger a radiative imbalance in Earth's energy budget that leads to both warming and cooling effects. These stem from carbon dioxide (CO_2) and non-CO_2 emissions, with the latter accounting for almost 70% of aviation's total effective radiative forcing (RF). Jointly, they equate to ∼4% of anthropogenic global warming (Kärcher 2018, Grewe *et al* 2019, Lee *et al* 2021). The aviation industry's recovery to near pre-pandemic levels (Boeing 2023) is a strong indication that this share will likely increase if mitigation measures are not implemented in time (Lee *et al* 2009). Here, we focus on nitrogen oxide (NO_x) emissions given their potential to instigate one of aviation's largest warming effects via short-term, indirect ozone (O_3) formation, a process that bears large uncertainty across NO_x-related processes (Lee

et al 2021). Furthermore, NO_x emissions can degrade air quality (Yim *et al* 2015, Quadros *et al* 2020) and are projected to outpace the growth in fuel consumption, making them a pressing concern, especially as they cannot be effectively mitigated even with the use of sustainable aviation fuels (Hamilton 2019). More efficient engine technologies also fall short in this regard as they often equate to larger pressure ratios and turbine inlet temperatures that reduce CO_2, but at the cost of increasing NO_x (Miller *et al* 2022, Quadros *et al* 2022a).

Varying the flight altitude, however, is an operationally feasible mitigation option for the near-term. Research has shown that flying lower within the upper troposphere and lower stratosphere (UTLS≡ here referring to altitudes between 9–12 km) leads, overall, to smaller non-CO_2 climate effects (Grewe *et al* 2002, Fichter *et al* 2005, Frömming *et al* 2012, Matthes *et al* 2021). Several of these studies, however, are limited, since their emission inventories were based on flight patterns from the early 2000s, when routes in the North American and European airspace represented roughly 80% of all air traffic (Gauss *et al* 2006, Skowron *et al* 2013, Søvde *et al* 2014, Matthes *et al* 2021). These analyses thus underrepresent spatial sensitivities of NO_x-O_3 climate effects in regions that are projected to grow in terms of air traffic, like Asia Pacific, thereby limiting their applicability to future aviation scenarios given aviation's spatially heterogeneous growth (Gössling and Humpe 2020, Airbus 2023).

To quantify such regional sensitivities to aviation-induced short-term NO_x-O_3 impacts, two main calculation methods are available: source apportionment (tagging) and sensitivity analysis (perturbation). The former estimates the contribution of different sources to a total pollutant concentration by labeling pertinent chemical species and tracking them across relevant reaction pathways, thereby guaranteeing a closed budget. The latter, on the other hand, is not additive and calculates the impact from an emission change using two simulations: one with a particular emission and another without (Grewe *et al* 2010, 2019, Grewe 2013, Mertens *et al* 2018, Thunis *et al* 2019). Here, we perform source apportionment via a tagging approach (Wang *et al* 2009, Grewe *et al* 2017, Rieger *et al* 2018) and conduct a sensitivity analysis (Blanchard 1999) via a perturbation method. If the relationship between emission and concentration is linear, then both methods yield identical results (Grewe *et al* 2010, Clappier *et al* 2017). Given the strong non-linearity of NO_x-O_3 chemistry (Cohan *et al* 2005, Grewe *et al* 2012), large differences ranging from a factor of 2–5 have been previously reported (Emmons *et al* 2012, Grewe *et al* 2012, 2019, Kranenburg *et al* 2013, Mertens *et al* 2018, Thunis *et al* 2019, Dedoussi *et al* 2020). These differences highlight each method's suitability to address distinct research questions. Tagging addresses 'what is a sector's contribution towards O_3?' while perturbation addresses 'what is the marginal impact of a sector on O_3 if its NO_x emissions are changed?'. Both questions should be addressed concurrently when assessing mitigation options for aviation's climate impact as it is insufficient to quantify a sector's contribution to total O_3 (tagging) without also gauging the impact of an emissions reduction (perturbation).

In this study, we use the ECHAM/ Modular Earth Sub-model System Cycle (MESSy) Atmospheric Chemistry (EMAC) model to compute the short-term O_3 produced from aviation NO_x for both methods. We run Eulerian and Lagrangian simulations, where the former calculates physical processes on an Earth-fixed frame and the latter along trajectories of advected air parcels (Brasseur and Jacob 2017). The computational cost of conducting the high-fidelity Eulerian tagging simulations increases significantly when having to analyze multiple emission scenarios. A more efficient approach to tagging is provided by the reduced-order Lagrangian sub-model AIRTRAC (supplement to Grewe *et al* 2014), which has been used to create the climate change functions (CCFs) (Grewe *et al* 2014, Frömming *et al* 2021) that estimate the climate impact of a local emission. With the upcoming requirement imposed by the European Union to include non-CO_2 effects in the monitoring, reporting and verifying initiative (MRV) (Scheelhaase *et al* 2024), AIRTRAC-derived CCFs could become an integral part of this reporting workflow. AIRTRAC is, however, limited by its simplified and linearized chemistry scheme, which is why we calculate correction factors to improve its accuracy.

This article has three main objectives: firstly, to understand how short-term NO_x-induced O_3 production from aviation and consequent RF vary geographically, altitudinally and seasonally, especially when compared to studies that assume present-day flight traffic distributions. Secondly, to quantify the differences between tagging and perturbation, which address distinct questions. We lastly compare the linearized Lagrangian tagging sub-model AIRTRAC with the non-linear TAGGING sub-model (Grewe *et al* 2017, Rieger *et al* 2018) to derive regional correction factors that can leverage AIRTRAC's computational efficiency for decision-making applications.

2. Methodology

We perform all simulations with the EMAC model (MESSy version 2.55.2) using three approaches: Eulerian tagging, perturbation and Lagrangian tagging. Overall, 74 simulations are run, totaling approximately 218 000 CPU hours. Altogether, these simulations currently form one of the most extensive datasets to assess short-term climate warming effects from aviation NO_x-induced O_3. The full dataset is openly available (Maruhashi *et al* 2023).

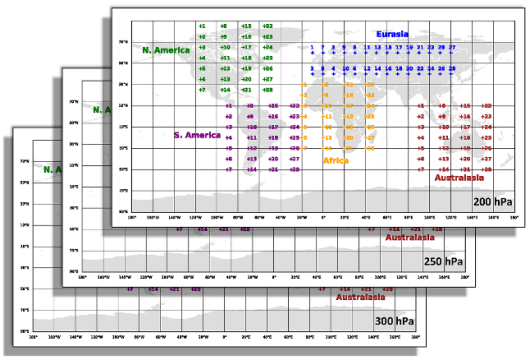

Figure 1. Geographic coordinates of all emission points at which 5×10^5 kg(NO) are emitted. Reproduced from Maruhashi *et al* (2022). CC BY 4.0.

2.1. The EMAC model

EMAC is a climate-chemistry model that comprises the Fifth Generation European Center for Medium-Range Weather Forecasts—Hamburg (ECHAM5) (Roeckner *et al* 2006) as its base general circulation model that can be linked via the MESSy Cycle 2 (MESSy2) interface to other sub-models. Common to all methods are the MECCA (Sander *et al* 2011), for background chemistry calculations, and the RAD sub-model (Dietmüller *et al* 2016), which estimates the instantaneous RF relative to the tropopause. Newtonian relaxation is used to nudge the sea surface temperature, the wind divergence, the vorticity and the logarithm of the sea-level pressure towards ERA-Interim reanalysis data corresponding to the simulation year. Lastly, all three methods have a common limitation: plume-scale chemical processes are disregarded, leading to a possible overestimation of the short-term O_3 impact by about 20%–30% (Meijer *et al* 1997, Kraabøl and Stordal 2000, Cameron *et al* 2013, Fritz *et al* 2020).

2.2. NO_x emissions

A pulse emission of 5×10^5 kg of nitric oxide (NO)[3] is introduced at 0600 UTC within a 15 min interval at each of the 28 points per region across five regions (North America, Eurasia, South America, Africa and Australasia) and three pressure altitudes (200, 250 and 300 hPa) on 1 January and July 2014. This NO emission per point represents on average ∼40% of total annual NO emissions by commercial aircraft flying over North America (Maruhashi *et al* 2022, Quadros *et al* 2022b). Each simulation tracks the production of O_3 from NO emitted on one of these two days for three months. The coordinates of all emission points (28 points × 5 regions × 3 altitudes = 420) are displayed in figure 1 (see section S1.1 of the supplement for exact coordinates). An overview of the methodology is provided in figure 2.

[3] Amount chosen for comparability with Grewe *et al* (2014)

2.3. Eulerian simulations

The Eulerian tagging method applies the TAGGING sub-model, which has been improved for this study by reducing the signal-to-noise ratio for small emissions (section S2 of the supplement). A set of 30 simulations based on the coordinates in figure 1 were performed, with an additional 12 simulations to assess the altitudinal variability of the O_3 production efficiency in North America for different NO emission amounts in July (section S3 of the supplement). The simulation setup resembles that of Jöckel *et al* (2016).

TAGGING is unable to independently consider multiple emission scenarios in parallel within one simulation since the chemical interaction between neighboring emissions is non-zero. Instead, due to computational constraints, each Eulerian simulation simultaneously emits NO at the 28 emission points per region. In doing so, however, we introduce interaction effects between emissions. The O_3 production efficiency from each Eulerian simulation, $O_{3,\mathrm{Net}}^{\mathrm{Eul}}$, is normalized by the emission amount of $28 \times 5 \times 10^5$ kg (NO).

This scaled mean Eulerian net O_3 production, $O_{3,\mathrm{Net}}^{\mathrm{Eul}}$ (equation (1)), includes seven production, five loss and one interaction term, which represents the non-linearity arising from interactions between emissions and saturation effects, $O_{3,\mathrm{Int}}$ (not explicitly part of the model output). The source-specific factor γ represents one of the main differences between tagging and perturbation as the former will scale the non-linear effects according to the mass contribution of each emission category (Clappier *et al* 2017, Matthes *et al* 2021). Further details in section S2 of the supplement.

$$O_{3,\mathrm{Net}}^{\mathrm{Eul}} = \frac{1}{\underbrace{28 \times 5 \times 10^5}_{\text{NO per simulation}}} \left(P_{HO_2} + P_{RO_2} + P_{OH} + P_{NO_y} + P_{HO_2NO_y} + P_{HO_2NMHC} + P_{OHNO_y} - L_{OH} - L_{HO_2} - L_{NO} - L_{RO} - L_{XO} + \gamma O_{3,\mathrm{Int}}\right). \quad (1)$$

The perturbation method is applied also using an Eulerian reference frame. The net O_3 produced using this approach is the difference between two simulations:

1. NO is simultaneously emitted at 28 points in figure 1, causing an NO disturbance of $28 \times \delta$NO, per region. Combining this with the background concentration, O_3^{REF}, the total O_3 field function becomes: $O_3\left(28 \times \delta\mathrm{NO} + O_3^{\mathrm{REF}}\right)$.
2. Additional reference simulation without any additional NO emissions. The O_3 field is the background O_3: O_3^{REF}. In total, two reference simulations are needed, one for each emission day (1 January and July).

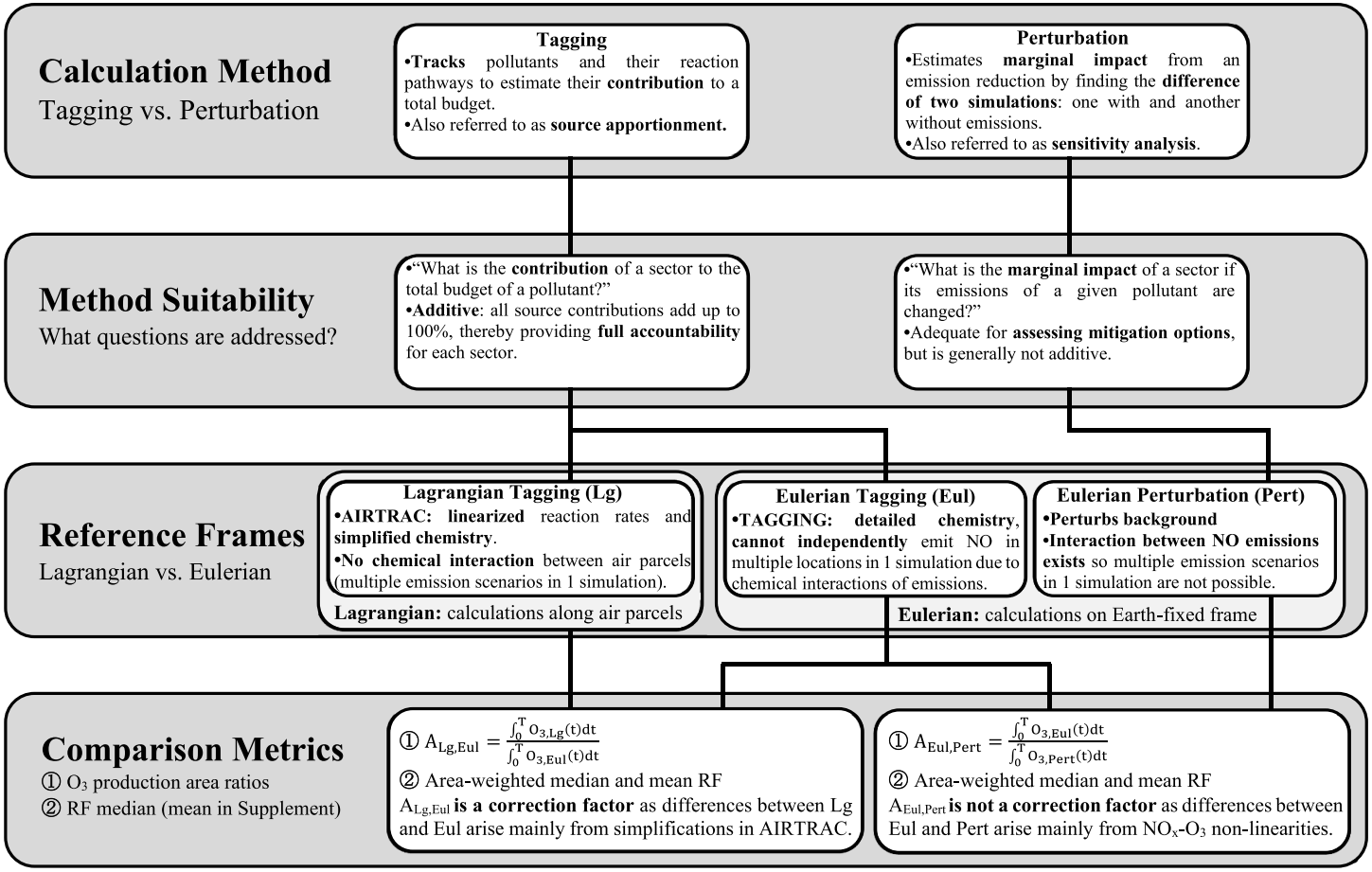

Figure 2. Summary of features across calculation methods (tagging and perturbation), questions addressed by each method, reference frames (Eulerian and Lagrangian) and comparison metrics (① area ratios of O_3 production efficiency curves and ② RF median (RF mean in supplement)).

The net O_3 production, $O_{3,\mathrm{Net}}^{\mathrm{Pert}}$, is given by equation (2), where a disturbance of δNO per emission point is introduced in the perturbed simulation that reflects the full chemical processes of EMAC. The result is normalized by the NO disturbance $28 \times 5 \times 10^5$ kg (NO):

$$O_{3,\mathrm{Net}}^{\mathrm{Pert}} = \frac{\overbrace{O_3\left(28 \times \delta\mathrm{NO} + O_3^{\mathrm{REF}}\right)}^{\text{Perturbed simulation}} - \overbrace{O_3^{\mathrm{REF}}}^{\text{Reference simulation}} + O_{3,\mathrm{Int}}}{\underbrace{28 \times 5 \times 10^5}_{\text{NO in perturbed simulation}}}. \tag{2}$$

We again acknowledge the existence of the interaction term $O_{3,\mathrm{Int}}$, however, unlike tagging, it attributes all non-linearities to the source from which the emission change is assumed to emanate, ergo $\gamma = 1$.

2.4. Lagrangian simulations

Lagrangian simulations are performed via a setup nearly identical to the one in Maruhashi *et al* (2022). AIRTRAC computes O_3 contributions from aviation NO_x emissions along air parcel trajectories via a tagging approach. An advantage of this sub-model is the possibility to simultaneously consider 28 emission scenarios in parallel within a single simulation, since there is no chemical interaction with neighboring NO_x emissions. This therefore makes it the most computationally efficient approach. It also allows for greater ease in the quantification of NO_x-O_3 uncertainties as more independent scenarios may be studied. As a shortcoming, however, the linearized reaction rates in AIRTRAC (constant O_3 production efficiency) and its simplified chemistry mechanism (fewer chemical processes tracked) are likely to provide less accurate estimates for the highly non-linear NO_x-O_3 chemistry. AIRTRAC uses only one production term from nitrogen compounds, P_{O3N}, and two loss terms: L_{O3N} (loss from nitrogen compounds) and L_{O3Y} (loss from non-nitrogen compounds) for each emission point. These are then averaged across the 28 emission points and normalized by the emitted NO (5×10^5 kg) to yield the Lagrangian net O_3 production from NO ($O_{3,\mathrm{Net}}^{\mathrm{Lg}}$), as shown in equation (3),

$$O_{3,\mathrm{Net}}^{\mathrm{Lg}} = \frac{1}{\underbrace{5 \times 10^5}_{\text{NO per simulation}}} \left(\overbrace{\sum_{i=1}^{28} \frac{P_{\mathrm{O3N},i} - L_{\mathrm{O3N},i} - L_{\mathrm{O3Y},i}}{28}}^{\text{Mean of 28 emission points}} \right). \tag{3}$$

To determine the contribution of the NO emission to atmospheric concentrations of active nitrogen species (NO_y), AIRTRAC scales the production and loss terms from relevant background species (e.g. HO_2) according to volume mixing ratio fractions computed by the tagging methodology of Grewe *et al* (2010), see section S4 of the supplement.

2.5. Method comparison metrics

To compare O_3 production efficiencies (i.e. emission-scaled O_3 production) across methods, the area ratios of their respective O_3 production efficiency curves as a function of time (i.e. O_3 curves) are evaluated. A_{M_1,M_2} (equation (4)), is defined in terms of two integrals: one for method 1 (M_1) and another for method 2 (M_2) being compared. M_1 and M_2 can correspond to Lagrangian tagging (Lg), Eulerian tagging (Eul), or the perturbation approach (Pert). The integration bounds encompass the full simulation period T of ~90 days. We refer to $A_{\mathrm{Lg,Eul}}$ as correction factors,

$$A_{M_1,M_2} = \frac{\int_0^T O_{3,M_1}(t)\,\mathrm{d}t}{\int_0^T O_{3,M_2}(t)\,\mathrm{d}t}. \tag{4}$$

We follow the RF definition of Maruhashi *et al* (2022), where it is expressed as the change in the net instantaneous long- and shortwave radiative fluxes from a pulse emission. Additionally, we scale down our RF estimates by a factor of 4 to make our estimate from a three-month pulse emission comparable to annual values from literature.

In all simulations, RF is computed online by the RAD sub-model and subsequently mapped to the climatological tropopause by the VISO sub-model (Jöckel *et al* 2010). To obtain a point estimate per scenario, we compute area-weighted medians, as they are unaffected by extreme values, thereby making them a more robust indicator. We additionally compute area- and time-averaged means (calculation method in section S5 of the supplement). To visualize the spread of the RF time series, we compute kernel density estimators (KDEs) for all cases (section S6 of the supplement).

3. Results and discussion

3.1. Comparison of O_3 production between methods

We first compare the O_3 production efficiency between the Eulerian tagging and perturbation methods. Figure 3(a) displays the case when NO is emitted at 300 hPa in North America during January. The former method (blue curve) leads to larger O_3 production when compared to the latter (orange curve). According to table 1, the Eulerian tagging estimates for this case are larger than the perturbation by a factor of 1.48. Across all simulations (see sections S7 and S8 of the supplement for all O_3 curves), we also find that Eulerian tagging is larger by a factor of $A_{\mathrm{Eul,Pert}}$ ranging from 1.16 to 2.55 with a mean of 1.83. This is consistent with past studies, where differences ranging from a factor of 2 to 5 were reported for road traffic and shipping (Grewe *et al* 2012, Mertens *et al* 2018) and around 1.6 for short-term aviation O_3 effects (Dahlmann *et al* 2011, Grewe *et al* 2019). The tagging method, however, will not always overestimate relative to the perturbation approach,

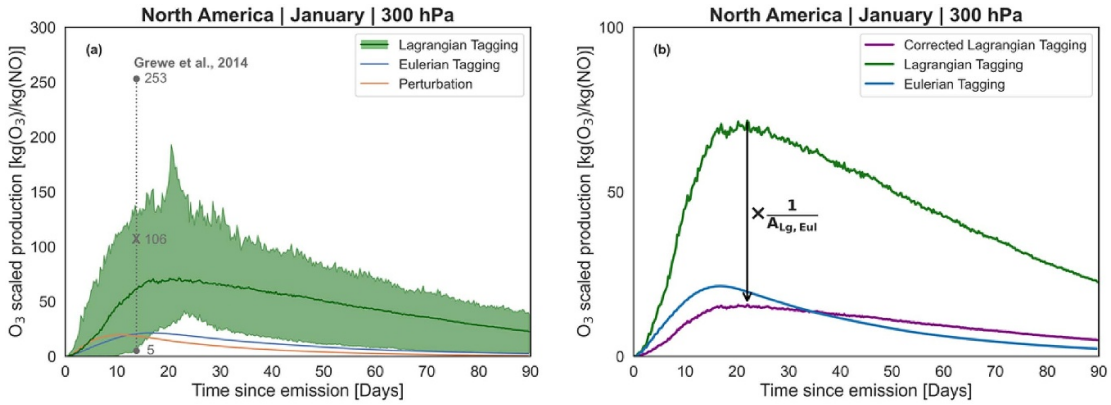

Figure 3. Normalized NO_x-induced O_3 production in North America. (a) Comparison between emission-scaled O_3 mass curves [kg(O_3)/kg(NO)] as estimated by the Lagrangian tagging (green), Eulerian tagging (blue) and perturbation (orange) methods for NO emitted at 300 hPa in January. The AIRTRAC and TAGGING sub-models were applied for the Lagrangian and Eulerian tagging methods, respectively. No specific sub-model is required for the perturbation method. The shaded green area represents the range of Lagrangian O_3 estimates for 28 independent emission scenarios based on the coordinates shown in figure 1. The green curve is the average of these 28 scenarios. The dotted gray line denotes the range of O_3 estimates (13.75 days after emission) obtained by Grewe *et al* (2014) using AIRTRAC to also study 5×10^5 kg of NO released at 200, 250, 300 and 400 hPa during 06h00, 12h00 and 18h00 UTC in January. The gray 'X' marks the mean value. (b) Application of the correction factor $A_{Lg,Eul} = 4.6$ from table 1 to the same emission scenario shown in (a). The green curve is the original O_3 estimated by the Lagrangian tagging curve, the purple curve is the corrected green curve and the blue curve is from the Eulerian tagging method.

Table 1. Calculation of the ratio of O_3 curve areas for the tagging and perturbation methods for all emission altitudes (200, 250 and 300 hPa), regions (NA = North America, SA = South America, EU = Eurasia, AF = Africa and AU = Australasia) and emission days (1 January and July 2014). Area ratios $A_{Lg,Eul}$ and $A_{Eul,Pert}$ refer to the application of equation (4) to the different methods (Lg = Lagrangian Tagging, Eul = Eulerian Tagging and Pert = Perturbation).

	Emission on 1 January 2014						Emission on 1 July 2014					
	$A_{Lg,Eul}$ [a]			$A_{Eul,Pert}$			$A_{Lg,Eul}$ [a]			$A_{Eul,Pert}$		
[hPa]	200	250	300	200	250	300	200	250	300	200	250	300
NA	2.38	3.62	4.59	2.10	1.74	1.48	1.71	2.17	2.23	2.55	2.37	2.27
SA	1.92	1.91	1.98	1.86	1.78	1.76	2.23	2.57	2.98	1.81	1.60	1.51
EU	2.62	4.38	5.91	2.07	1.44	1.16	1.68	1.99	2.68	2.38	2.34	2.04
AF	1.97	2.08	2.40	1.93	1.92	1.90	2.26	2.70	3.44	1.90	1.78	1.66
AU	1.96	1.98	2.03	1.60	1.62	1.64	2.50	3.20	3.81	1.70	1.53	1.38

[a] Correction factors refer specifically to $A_{Lg,Eul}$ as they consider differences between the tagging methods arising from the limitations of AIRTRAC. These factors then enable AIRTRAC to more accurately calculate 28 independent emission scenarios in a single simulation.

this ultimately depends on the type of linearity underlying the studied phenomenon (Grewe *et al* 2010). Thunis *et al* (2019) and Dedoussi *et al* (2020), for instance, found larger values by a factor of up to 3 for the perturbation approach when considering ground-level particulate matter ($PM_{2.5}$). Such differences are due to a combination of non-linear compensation effects arising from other emissions sources, where total O_3 non-linearities are either shared across individual sources (tagging) or are fully allocated to a single source (perturbation), oftentimes by means of distinct reaction rates (Emmons *et al* 2012, Grewe *et al* 2012, Matthes *et al* 2021).

Differences between Lagrangian and Eulerian tagging sub-models, are however, mainly attributable to AIRTRAC's simplifications. The green shaded area indicates the range of O_3 estimates from 28 independent emission scenarios considered by the Lagrangian approach, contrasting with only one scenario of the Eulerian alternative. Likely, the difference by a factor of 4.6 between the areas of the green and blue O_3 curves in figure 3(a) arises from the lack of chemical interaction between Lagrangian air parcels ($O_{3,Int} = 0$), simplified chemistry and AIRTRAC's linearized reaction rates that translate to constant O_3 production efficiencies. Unlike the Eulerian tagging and perturbation methods, where O_3 production efficiencies vary with the amount of emitted NO, AIRTRAC's O_3 production efficiency is invariant to emission strength (i.e. amount emitted, see section S3 of supplement). This equates to discarding shifts in the local NO_x regime from varying the amount of NO emitted as there is no feedback between emission and background. However, to leverage the computational efficiency of AIRTRAC despite these simplifications, we derive correction factors $A_{Lg,Eul}$ in table 1. Figure 3(b) illustrates the application of a correction factor ($A_{Lg,Eul} = 4.6$) for the scenario

of figure 3(a), where the corrected Lagrangian curve (purple) now more closely resembles the Eulerian tagging curve (blue). More simulations would be required, however, to capture O_3 behavior in other aviation emission scenarios considered in Grewe *et al* (2014), as is indicated by the gray line in figure 3(a).

3.2. Altitudinal variation of short-term RF from aviation NO_x-O_3 interactions

The variation between short-term O_3 median RF from aviation NO_x with emission altitude for all three methods is presented in figure 4. For the Eulerian tagging and perturbation methods, emitting at higher altitudes always leads to a larger median RF per Tg (N). The Lagrangian tagging method also largely predicts a similar relation, but displays some cases of inversions, e.g. in North America the RF is largest at 250 hPa. Frömming *et al* (2021) also report a non-monotonic relation with altitude for aviation's net NO_x warming effect using AIRTRAC while Matthes *et al* (2021), via a multi-model approach involving EMAC, also found a non-monotonic relation for lower altitudes (∼300 hPa). One of the inversions in figure 4(a), for instance, may be explained by larger O_3 production efficiency maxima occurring at 250 hPa during January for North America (see figure S7.1(b) in the supplement). The predominant trend, however, is to witness warming effects from aircraft NO_x emissions increase with altitude within the troposphere, as there is a more efficient accumulation of NO at higher altitudes from fewer removal processes (Grewe *et al* 2002, Köhler *et al* 2008, Frömming *et al* 2012, Matthes *et al* 2021).

We note significant regional and seasonal variations in the estimated RF. During January, figure 4(a) presents larger values in the southern hemisphere (SA, AF and AU) while in July (figure 4(b)), warming in NA and EU increases, but decreases for the remaining three southern regions. Such a seasonal shift occurs from the strong photochemical dependence of O_3 production (Stevenson *et al* 2004, Gauss *et al* 2006, Frömming *et al* 2021, Maruhashi *et al* 2022). Seasonality also significantly impacts the altitudinal sensitivity of O_3 RF. Flying higher in Eurasia during January from 250 to 200 hPa leads to an increase in short-term O_3 warming by ∼20% according to the Eulerian tagging approach (figure 4(a)). In July, the same altitudinal shift would lead to an increase of 50% (figure 4(b)). This suggests that altitudinal measures for the short-term mitigation of NO_x-O_3 impacts are most effective during the local summer. Across all methods, Australasia generates the largest RF for a January emission (as is also seen by the wider spread of the RF KDEs in section 6 of the supplement), which is explained by the lower background NO concentrations in its vicinity (Gilmore *et al* 2013, Skowron *et al* 2015, Maruhashi *et al* 2022).

Comparing our RF perturbation estimates in figure 4 with Lee *et al* (2021) reveals regional differences, particularly for low-altitude emissions in North America and Eurasia. For a January emission at 300 hPa in North America (figure 4(a)), for example, our RF value is smaller by a factor of 3 relative to their lower bound estimate of 16 (mW m^{-2})/Tg (N). When juxtaposed with Eulerian tagging estimates by Matthes *et al* (2021), our Eulerian tagging results from July emissions (figure 4(b)) compare well, albeit with larger discrepancies observed at the highest emission altitude. Even larger differences of a factor of 2 emerge when comparing our Eulerian tagging estimates with Matthes *et al* (2021) for January in Southern regions (SA and AU). Our study therefore underscores that estimates based on global emission inventories, if used to evaluate the effects of increasing emissions in underrepresented regions, could over- or underestimate aviation NO_x-O_3 warming impacts depending on the region and method. A robust, global assessment of aviation's evolving non-CO_2 effects should take into account the dynamic shift in air traffic distribution given the heterogeneity in regional NO_x-O_3 responses.

These disparities also bring to light the large uncertainties surrounding aviation NO_x-O_3 effects that arise from distinct methods and may increase further from adopting additional model types like chemical-transport models (CTMs) or climate-response models (CRMs) (Cameron *et al* 2017). Comparison with our mean RF values leads to similar conclusions (section S9 of supplement). Relative to our tagging estimates, we lastly note that TAGGING consistently exhibits larger RF in Pacific regions when compared to AIRTRAC, which may explain some magnitude differences in figure 4. During a northern emission in January for instance, TAGGING estimates larger warming in the southern Pacific relative to AIRTRAC (figures S10.1(d)–(f) and (j)–(l) of the supplement), leading to smaller differences between their RF estimates for NA and EU in figure 4(a).

Figure 4 should also be interpreted in terms of the distinct research questions that the tagging and perturbation approaches address. Eulerian tagging is represented by the black line and indicates aviation's sectoral contribution to the overall O_3 budget and how this varies with altitude, region and season. In figure 4(b), for instance, flying higher from 250 to 200 hPa in Eurasia could lead to a strong increase in aviation's contribution to total O_3 via an increase in its short-term O_3 production, assuming the amount emitted by other sectors is unchanged. In contrast, perturbation (shown in blue) investigates the impact on RF that would result at each corresponding scenario if aviation emissions were regionally increased by 28 × 0.5 Gg. A discussion of how to combine these two methods is found in Mertens *et al* (2018).

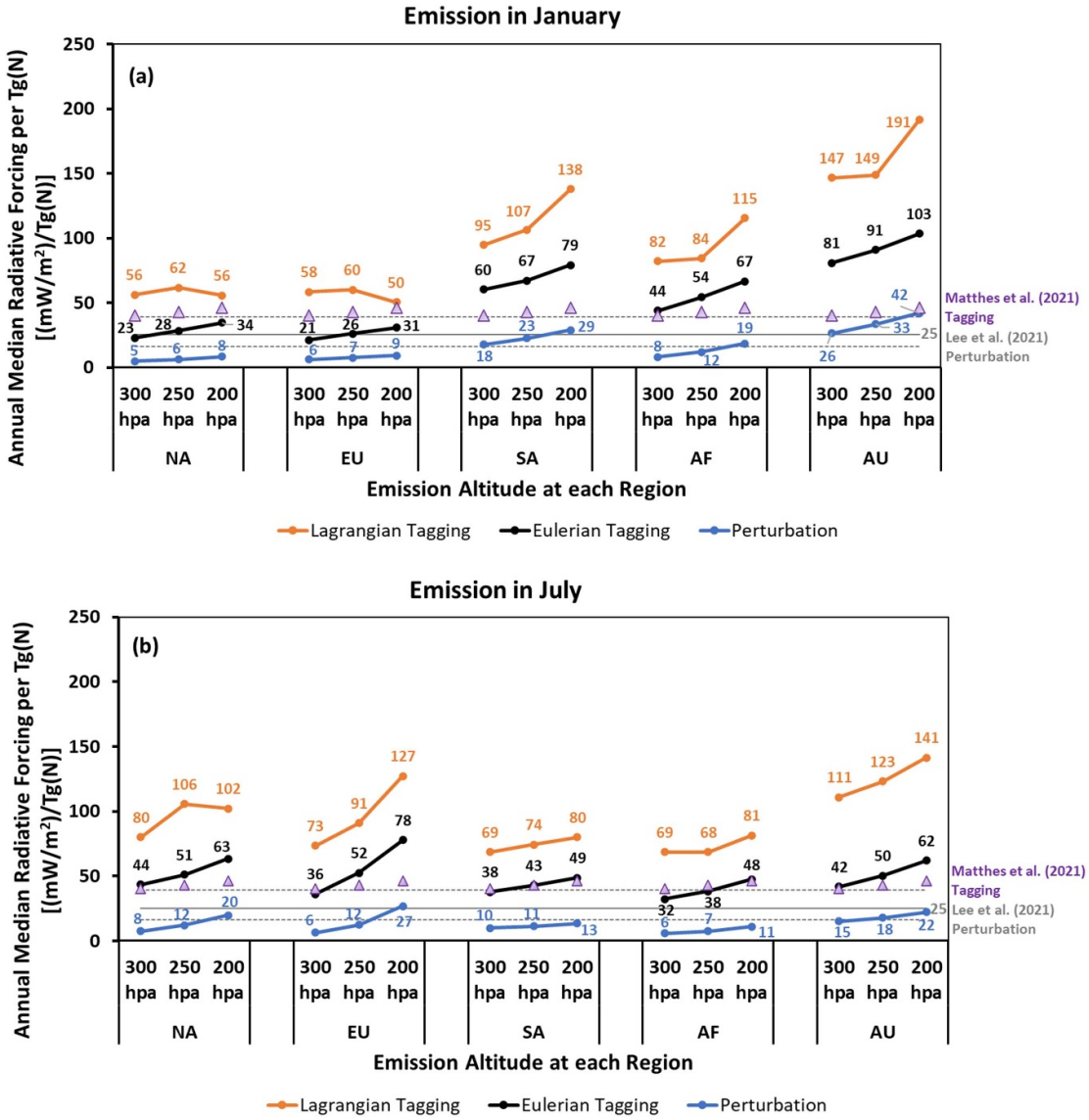

Figure 4. Annualized, area-weighted median radiative forcing point estimates (section S5 of supplement for calculation method) from short-term NO_x-induced O_3 for emission altitudes of 300 hPa (∼9.2 km), 250 hPa (∼10.4 km) and 200 hPa (∼11.8 km) across all five regions (North America (NA), South America (SA), Eurasia (EU), Africa (AF) and Australasia (AU)) during (a) 1 January and (b) 1 July of 2014. The solid gray line represents the corresponding mean RF estimate for short-term O_3 effects from Lee *et al* (2021) using a perturbation approach. The dotted gray lines demarcate the 90% confidence interval of the same study, where the 5% lower limit is 16 and the 95% upper limit is 39 mW m^{-2}. The purple triangles depict the tagging estimates in mWm^{-2} of Matthes *et al* (2021), who calculated 43 for a base flight altitude (equated to our 250 hPa), 46 for a *flying higher* and 40 for a *flying lower* scenario, which were compared to our 200 and 300 hPa estimates, respectively. For clarity, these values are not labeled above. All RF estimates presented in (a) and (b) have been scaled to represent the equivalent value of a 1 Tg of nitrogen (N) emission.

4. Summary and conclusions

The variation between aircraft NO_x emission altitude and short-term climate warming from O_3 production has been assessed using three methods (Eulerian tagging, perturbation and Lagrangian tagging), all within the framework of the EMAC model. We performed 74 simulations across five regions and three altitudes during the summer and winter seasons to account for seasonal and regional differences. This study does not include NO_x terms that lead to a reduced warming, which, when combined with the short-term O_3 warming component, may lead to a negative net-NO_x forcing (Holmes *et al* 2011, Terrenoire *et al* 2022).

In the process, differences between estimates from these approaches were discussed, in the context of the questions that they can be used to answer, and a set of correction factors $A_{Lg,Eul}$ (table 1) was calculated for the widely-used Lagrangian AIRTRAC sub-model (used in e.g. CCFs (Grewe *et al* 2014, Frömming *et al* 2021)) that may be useful for Europe's new MRV initiative.

Our results regarding the altitudinal relationship of aircraft climate effects from short-term NO_x-O_3 interactions only partly confirm past studies, which

conducted their analyses based on emission inventories that are influenced by more numerous flights in the Northern Trans-Atlantic. Their approach may still significantly underestimate the altitudinal sensitivity of RF for Southern regions, like Australasia, particularly for emissions in January. We have, however, verified that the proportional relationship between O_3 RF and altitude holds regionally for all five regions during both seasons according to the Eulerian tagging and perturbation approaches. A few exceptions were found for the Lagrangian method, but certain non-monotonic trends have also been found in earlier studies (Frömming *et al* 2021, Matthes *et al* 2021). We have also found that the change in short-term O_3 RF with altitude is more impactful when flying higher (or lower) during the season in which greater solar radiation is available.

Differences between the Eulerian tagging and perturbation approaches range from a factor of 1.16 to 2.55 with a mean of 1.83 for the O_3 mass curves. These estimates agree well with the range of 2–5 provided by literature (Emmons *et al* 2012, Grewe *et al* 2012, 2019, Kranenburg *et al* 2013, Mertens *et al* 2018, Thunis *et al* 2019, Dedoussi *et al* 2020, Matthes *et al* 2021). The Lagrangian tagging sub-model exhibits larger differences likely due to a combination of reasons: the lack of inter-parcel chemical interaction effects, the relatively simplified chemistry scheme and the linearization of the NO_x-O_3 response. To correct for these shortcomings, we compute and provide correction factors.

Although O_3 mass estimates from tagging and perturbation methods can differ by almost a factor of 3, both should still be considered in tandem for a comprehensive assessment of aviation climate effects, given that they address distinct questions. Each of the three methods presented here can play a unique role in the mitigation decision-making process. Tagging identifies mitigation opportunities by determining the share of each sector to the total O_3 budget. The perturbation method may be applied to evaluate an emissions reduction measure of a certain sector. Lastly, the corrected Lagrangian tagging method can help us efficiently gauge the uncertainty levels in these estimates by providing more data for more scenarios and better understand transport-related phenomena (Maruhashi *et al* 2022). When addressing technological, operational or regulatory decisions, these methods would provide valuable, complementary insights.

Data availability statement

The simulation data produced and analyzed for this assessment are openly available in the following repository: https://doi.org/10.4121/56327667-69f1-4340-be45-9f9a6bd80584.

Acknowledgments

We would like to express our gratitude to Anke Roiger from DLR (German Aerospace Center) for providing valuable feedback. This research used the Dutch national e-infrastructure with the support of the SURF Cooperative (Grant Nos. EINF-441 and EINF-2734) as well as resources from the Deutsches Klimarechenzentrum (DKRZ) granted by its Scientific Steering Committee (WLA) under project ID bd1063.

Funding

This research is embedded within the ACACIA (Advancing the Science for Aviation and Climate; www.acacia-project.eu) project, which is funded by the European Commission, Horizon 2020 Framework Programme (ACACIA under the Grant No. 875036).

ORCID iDs

Jin Maruhashi https://orcid.org/0000-0003-2667-4161
Mariano Mertens https://orcid.org/0000-0003-3549-6889
Volker Grewe https://orcid.org/0000-0002-8012-6783
Irene C Dedoussi https://orcid.org/0000-0002-8966-9469

References

Airbus 2023 Global market forecast 2023–2042 (available at: www.airbus.com/en/products-services/commercial-aircraft/market/global-market-forecast) (Accessed 25 August 2023)
Blanchard C L 1999 Methods for attributing ambient air pollutants to emission sources *Annu. Rev. Environ. Resour.* **24** 329–65
Boeing 2023 Commercial market outlook (available at: www.boeing.com/commercial/market/commercial-market-outlook) (Accessed 21 August 2023)
Brasseur G and Jacob D 2017 Model equations and numerical approaches *Modeling of Atmospheric Chemistry* (Cambridge University Press) pp 84–204
Cameron M A *et al* 2017 An intercomparative study of the effects of aircraft emissions on surface air quality *J. Geophys. Res. Atmos.* **122** 8325–44
Cameron M A, Jacobson M Z, Naiman A D and Lele S K 2013 Effects of plume-scale versus grid-scale treatment of aircraft exhaust photochemistry *Geophys. Res. Lett.* **40** 5815–20
Clappier A, Belis C A, Pernigotti D and Thunis P 2017 Source apportionment and sensitivity analysis: two methodologies with two different purposes *Geosci. Model Dev.* **10** 4245–56
Cohan D S, Hakami A, Hu Y and Russell A G 2005 Nonlinear response of ozone to emissions: source apportionment and sensitivity analysis *Environ. Sci. Technol.* **39** 6739–48
Dahlmann K, Grewe V, Ponater M and Matthes S 2011 Quantifying the contributions of individual NO_x sources to the trend in ozone radiative forcing *Atmos. Environ.* **45** 2860–8

Dedoussi I C, Eastham S D, Monier E and Barrett S R H 2020 Premature mortality related to United States cross-state air pollution *Nature* **578** 261–5
Dietmüller S *et al* 2016 A new radiation infrastructure for the modular Earth submodel system (MESSy, based on version 2.51) *Geosci. Model Dev.* **9** 2209–22
Emmons L K, Hess P G, Lamarque J-F and Pfister G G 2012 Tagged ozone mechanism for MOZART-4, CAM-chem and other chemical transport models *Geosci. Model Dev.* **5** 1531–42
Fichter C, Marquart S, Sausen R and Lee D S 2005 The impact of cruise altitude on contrails and related radiative forcing *Meteorol. Z.* **14** 563–72
Fritz T M, Eastham S D, Speth R L and Barrett S R H 2020 The role of plume-scale processes in long-term impacts of aircraft emissions *Atmos. Chem. Phys.* **20** 5697–727
Frömming C, Grewe V, Brinkop S, Jöckel P, Haslerud A S, Rosanka S, van Manen J and Matthes S 2021 Influence of weather situation on non-CO_2 aviation climate effects: the REACT4C climate change functions *Atmos. Chem. Phys.* **21** 9151–72
Frömming C, Ponater M, Dahlmann K, Grewe V, Lee D S and Sausen R 2012 Aviation-induced radiative forcing and surface temperature change in dependency of the emission altitude *J. Geophys. Res. Atmos.* **117** D19104
Gauss M, Isaksen I S A, Lee D S and Søvde O A 2006 Impact of aircraft NO_x emissions on the atmosphere—tradeoffs to reduce the impact *Atmos. Chem. Phys.* **6** 1529–48
Gilmore C K, Barrett S R H, Koo J and Wang Q 2013 Temporal and spatial variability in the aviation NO_x-related O_3 impact *Environ. Res. Lett.* **8** 034027
Gössling S and Humpe A 2020 The global scale, distribution and growth of aviation: implications for climate change *Glob. Environ. Change* **65** 102194
Grewe V 2013 A generalized tagging method *Geosci. Model Dev.* **6** 247–53
Grewe V *et al* 2014 Aircraft routing with minimal climate impact: the REACT4C climate cost function modelling approach (V1.0) *Geosci. Model Dev.* **7** 175–201
Grewe V, Dahlmann K, Matthes S and Steinbrecht W 2012 Attributing ozone to NO_x emissions: implications for climate mitigation measures *Atmos. Environ.* **59** 102–7
Grewe V, Dameris M, Fichter C and Lee D S 2002 Impact of aircraft NO_x emissions. Part 2: effects of lowering the flight altitude *Meteorol. Z.* **11** 197–205
Grewe V, Matthes S and Dahlmann K 2019 The contribution of aviation NO_x emissions to climate change: are we ignoring methodological flaws? *Environ. Res. Lett.* **14** 121003
Grewe V, Tsati E and Hoor P 2010 On the attribution of contributions of atmospheric trace gases to emissions in atmospheric model applications *Geosci. Model Del.* **3** 487–99
Grewe V, Tsati E, Mertens M, Frömming C and Jöckel P 2017 Contribution of emissions to concentrations: the TAGGING 1.0 submodel based on the Modular Earth Submodel System (MESSy 2.52) *Geosci. Model Dev.* **10** 2615–33
Hamilton B A 2019 Alternative jet fuels emissions, quantification methods creation and validation report *Publication Final Report for ACRP Project 02–80* (*McLean, Virginia*) p 122
Holmes C D, Tang Q and Prather M J 2011 Uncertainties in climate assessment for the case of aviation NO *Proc. Natl Acad. Sci. USA* **108** 10997–1002
Jöckel P, Kerkweg A, Pozzer A, Sander R, Tost H, Riede H, Baumgaertner A, Gromov S and Kern B 2010 Development cycle 2 of the modular Earth submodel system (MESSy2) *Geosci. Model Dev.* **3** 717–52
Jöckel P, Scharffe D and Zahn A 2016 Earth system chemistry integrated modelling (ESCiMo) with the Modular Earth Submodel System (MESSy) version 2.51 *Geosci. Model Dev.* **9** 1153–200
Kärcher B 2018 Formation and radiative forcing of contrail cirrus *Nat. Commun.* **9** 1824
Köhler M O, Rädel G, Dessens O, Shine K P, Rogers H L, Wild O and Pyle J A 2008 Impact of perturbations to nitrogen oxide emissions from global aviation *J. Geophys. Res.* **113** D11305
Kraabøl A G and Stordal F 2000 Modelling chemistry in aircraft plumes 2: the chemical conversion of NO_x to reservoir species under different conditions *Atmos. Environ.* **34** 3951–62
Kranenburg R, Segers A J, Hendriks C and Schaap M 2013 Source apportionment using LOTOS-EUROS: module description and evaluation *Geosci. Model Dev.* **6** 721–33
Lee D S *et al* 2021 The contribution of global aviation to anthropogenic climate forcing for 2000–2018 *Atmos. Environ.* **244** 117834
Lee D S, Fahey D W, Forster P M, Newton P J, Wit C N, Lim L L, Owen B and Sausen R 2009 Aviation and global climate change in the 21st century *Atmos. Environ.* **43** 3520–37
Maruhashi J, Grewe V, Frömming C, Jöckel P and Dedoussi I C 2022 Transport patterns of global aviation NO_x and their short-term O_3 radiative forcing—a machine learning approach *Atmos. Chem. Phys.* **22** 14253–82
Maruhashi J, Mertens M, Grewe V and Dedoussi I C 2023 Supplementary dataset for "A multi-method assessment of the regional sensitivities between flight altitude and short-term O_3 climate warming from aircraft NO_x emissions" 4TU ResearchData (https://doi.org/10.4121/56327667-69f1-4340-be45-9f9a6bd80584)
Matthes S *et al* 2021 Mitigation of non-CO_2 aviation's climate impact by changing cruise altitudes *Aerospace* **8** 36
Meijer E W, Van Velthoven P F, Wauben W M, Beck J P and Velders G J 1997 The effects of the conversion of nitrogen oxides in aircraft exhaust plumes in global models *Geophys. Res. Lett.* **24** 3013–6
Mertens M, Grewe V, Rieger V S and Jöckel P 2018 Revisiting the contribution of land transport and shipping emissions to tropospheric ozone *Atmos. Chem. Phys.* **18** 5567–88
Miller C J, Prashanth P, Allroggen F, Grobler C, Sabnis J S, Speth R L and Barrett S R H 2022 An environmental cost basis for regulating aviation NO_x emissions *Environ. Res. Commun.* **4** 055002
Quadros F D A, Snellen M and Dedoussi I C 2020 Regional sensitivities of air quality and human health impacts to aviation emissions *Environ. Res. Lett.* **15** 105013
Quadros F D A, Snellen M and Dedoussi I C 2022a Recent and projected trends in global civil aviation fleet average NO_x emissions indices *AIAA SCITECH 2022 Forum* pp 2022–51
Quadros F D A, Snellen M, Sun J and Dedoussi I C 2022b Global civil aviation emissions estimates for 2017–2020 using ADS-B data *J. Aircr.* **59** 1394–405
Rieger V S, Mertens M and Grewe V 2018 An advanced method of contributing emissions to short-lived chemical species (OH and HO_2): the TAGGING 1.1 submodel based on the Modular Earth Submodel System (MESSy 2.53) *Geosci. Model Dev.* **11** 2049–66
Roeckner E *et al* 2006 Sensitivity of simulated climate to horizontal and vertical resolution in the ECHAM5 atmosphere model *J. Clim.* **19** 3771–91
Sander R *et al* 2011 The atmospheric chemistry box model CAABA/MECCA-3.0 *Geosci. Model Dev.* **4** 373–80
Scheelhaase J, Grimme W and Maertens S 2024 EU trilogue results for the aviation sector – key issues and expected impacts *Transp. Res. Procedia* **78** 206–14
Skowron A, Lee D S and De León R R 2015 Variation of radiative forcings and global warming potentials from regional aviation NO_x emissions *Atmos. Environ.* **104** 69–78
Skowron A, Lee D S and León R R D 2013 The assessment of the impact of aviation NO_x on ozone and other radiating forcing responses—the importance of representing cruise altitudes accurately *Atmos. Environ.* **74** 159–68
Søvde O, Matthes S, Skowron A, Iachetti D, Lim L, Owen B, Hodnebrog T, Di Genova G, Pitari G and Lee D 2014 Aircraft emission mitigation by changing route altitude: a

multi-model estimate of aircraft NO_x emission impact on O_3 photochemistry *Atmos. Environ.* **95** 468–79
Stevenson D S, Doherty R M, Sanderson M G, Collins W J, Johnson C E and Derwent R G 2004 Radiative forcing from aircraft NO_x emissions: mechanisms and seasonal dependence *J. Geophys. Res.* **109** D17307
Terrenoire E, Hauglustaine D A, Cohen Y, Cozic A, Valorso R, Lefèvre F and Matthes S 2022 Impact of present and future aircraft NO_x and aerosol emissions on atmospheric composition and associated direct radiative forcing of climate *Atmos. Chem. Phys.* **22** 11987–2023
Thunis P *et al* 2019 Source apportionment to support air quality planning: strengths and weaknesses of existing approaches *Environ. Int.* **130** 104825
Wang Z S, Chien C J and Tonnesen G S 2009 Development of a tagged species source apportionment algorithm to characterize three-dimensional transport and transformation of precursors and secondary pollutants *J. Geophys. Res.* **114** D21206
Yim S H L, Lee G L, Lee I H, Allroggen F, Ashok A, Caiazzo F, Eastham S D, Malina R and Barrett S R H 2015 Global, regional and local health impacts of civil aviation emissions *Environ. Res. Lett.* **10** 034001